Journal of Computational Interdisciplinary Sciences (2012) 3(1-2): 87-98
© 2012 Pan-American Association of Computational Interdisciplinary Sciences
Printed version ISSN 1983-8409 / Online version ISSN 2177-8833
http://epacis.net
doi: 10.6062/jcis.2012.03.02.0054

Complex spatio-temporal dynamics in metal electrodissolution: three dimensional cell geometry models

Adrian Bîrzu[1] and Vilmos Gáspár[2]

Manuscript received on May 29, 2012 / accepted on August 28, 2012

ABSTRACT

Complex dynamics of current distribution on ring or disk working electrodes is studied numerically by modelling metal electrodissolution under potentiostatic control in a three dimensional electrochemical cell. Such spatially distributed systems exhibit extremely rich dynamics in the oscillatory regime, ranging from rotating pulses to spatio-temporal chaos. Several dynamical behaviors were selected and characterized using the Karhunen-Loève (KL) decomposition and the analytical signal approach.

Keywords: spatially extended systems, nonlinear dynamics, electrochemical systems, proper orthogonal decomposition, and analytical signal approach.

1 INTRODUCTION

Electrochemical systems are ideal candidates for the study of nonlinear processes. A typical example is the electrodissolution of metals: the corresponding evolution equations are nonlinear and the working electrode (WE) can be easily maintained far from the thermodynamic equilibrium, using for example potentiostatic control, when the voltage between the working and a reference electrode (RE) is kept constant [1, 2]. Since 1990, the experimental and theoretical study of spatially distributed nonlinear electrochemical system flourished [1-5]. A fruitful alternative of study was to use large arrays of electrochemical oscillators [6, 7].

Theoretically, the state of a spatially extended nonlinear system is characterized by an infinite number of degrees of freedom [8]. This leads to a great richness of dynamical behaviours compared to point-like systems that calls for complex methods for characterization of the spatio-temporal dynamics. This article presents two such relevant methods: the Karhunen-Loève (KL) decomposition and the analytical signal approach, based on the Hilbert transform.

2 THE MODEL AND THE ANALYSIS OF THE DYNAMICS

We employ a generic model that describes qualitatively the electrodissolution of a metal that under certain conditions may show passivity [9]. The geometries of the electrochemical cell are depicted in Figures 1a and b. In both cases, the WE (either a ring, Fig. 1a, or a disk, Fig. 1b, embedded in an insulator) is placed on the bottom of the cell. On the top of the cell there is a ring-shaped counter electrode (CE), while the reference electrode is considered as point-like.

The main dynamic variable is the electrostatic potential in the electrolyte. For the usual experimental values of the electrolyte concentration in such setup, the electroneutrality condition holds and the Laplace equation is valid in the electrolyte:

$$\nabla^2\phi = 0 \qquad (1)$$

Correspondence to: Adrian Birzu – E-mail: abirzu@uaic.ro
[1] Department of Chemistry, Al. I. Cuza University, Blvd. Carol I no. 11, 700506, Iaşi, Romania
[2] Department of Physical Chemistry, University of Debrecen, H-4032 Debrecen, Egyetem tér 1, Hungary

In cylindrical coordinates this reads:

$$\frac{\partial^2\phi}{\partial\rho^2}+\frac{1}{\rho}\frac{\partial\phi}{\partial\rho}+\frac{1}{\rho^2}\frac{\partial^2\phi}{\partial\theta^2}+\frac{\partial^2\phi}{\partial z^2}=0 \tag{2}$$

where ϕ is the electrostatic potential at a point described by the cylindrical coordinates (ρ, θ, z).

The boundary condition at the WE is the charge balance equation, which gives a time dependent state:

$$\sigma\frac{\partial\phi}{\partial z}\Big|_{\mathrm{WE}}=C_{\mathrm{DL}}\frac{\partial\phi}{\partial t}\Big|_{\mathrm{WE}}-\frac{A}{e^{-\alpha(-\phi_{\mathrm{DL}}+E_{\mathrm{F}})}+1} \tag{3}$$

Here the left hand term represents the total current density at the WE. The first term in the right hand side gives the capacitive current, while the second term is the reaction current for which a smoothed Heaviside function was used. σ is the electrolyte conductivity (considered constant), C_{DL} is the capacitance of the electric double layer in front of the WE per unit area, A and α are constants, ϕ_{DL} is the potential drop over the double layer and E_{F} is the active-passive transition potential (Flade potential). It is considered to be a linear function of the pH of the electrolyte in front of the WE:

$$E_{\mathrm{F}}=F_1+F_2\log[\mathrm{H}^+]_{\mathrm{WE}} \tag{4}$$

F_1 and F_2 are constants.

The insulator from the plane of the WE, the lateral wall and the inner region of the CE are modeled by no-flux boundary conditions. The metal of the WE is considered as reference and consequently the potential at the reference electrode equals the applied voltage:

$$\phi\big|_{\mathrm{RE}}=V_{\mathrm{apl}} \tag{5}$$

At the CE, linear kinetics is assumed and the capacitive current is neglected:

$$-\sigma\frac{\partial\phi}{\partial z}\Big|_{\mathrm{CE}}=k\left(\phi\big|_{\mathrm{CE}}-\phi^{\mathrm{CE}}_{\mathrm{Metal}}\right)$$

The balance equation for the protons in front of the WE is the following:

$$\begin{aligned}\frac{\partial[\mathrm{H}^+]_{\mathrm{WE}}}{\partial t} &= \frac{2D\left([\mathrm{H}^+]_{\mathrm{bulk}}-[\mathrm{H}^+]_{\mathrm{WE}}\right)}{\delta^2}\\ &\quad+\frac{2\mu[\mathrm{H}^+]_{\mathrm{WE}}}{\delta}\frac{\partial\phi}{\partial z}\Big|_{\mathrm{WE}}\end{aligned} \tag{6}$$

The pH at the WE changes due to diffusion and migration; linear distribution is assumed for proton concentration in the diffusion layer in front of the WE. Here D is the diffusion coefficient of the protons, μ is the migration coefficient, δ is the thickness of the diffusion layer and $[\mathrm{H}^+]_{\mathrm{bulk}}$ is the proton concentration in the bulk of the electrolyte (considered to be constant).

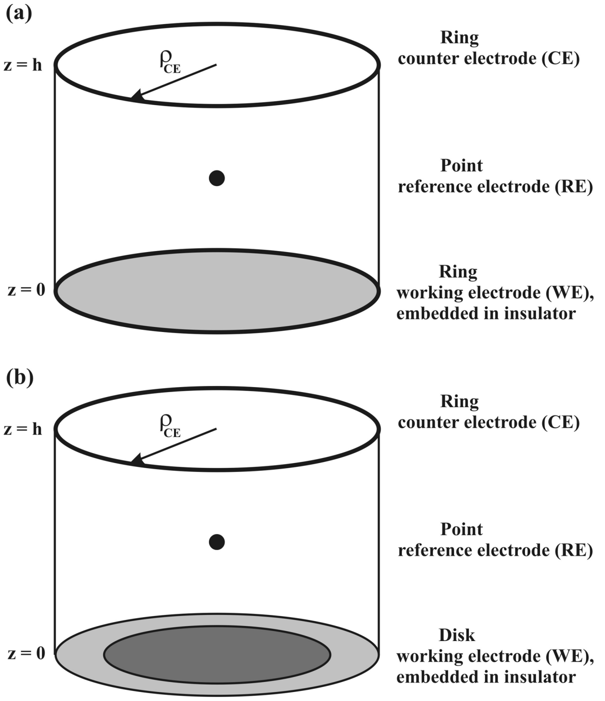

Figure 1 – Geometries of the electrochemical cell.

Numerical solution

The elliptic partial differential equation (2) with the above mentioned boundary conditions was solved numerically using a finite difference method on a cylindrical grid. The integration in time for the time dependent boundary conditions (3) and (6) was done with a 4th order Runge-Kutta algorithm. The sparse algebraic system resulting from the finite difference discretisation was solved using ma28 or ma48 routines from Harwell library [10] at each time integration step. The resulting dynamics at the ring and disk WE was analyzed using mainly two methods: the KL decomposition and the analytical signal approach. We shall give below a brief presentation of these methods.

A. Karhunen-Loève (KL) decomposition

This is a powerful tool to characterize the spatially extended dynamical systems which are called also, especially in engineering applications, distributed parameter systems. A general mathematical description of the method can be found in [11], while details regarding practical numerical implementations are given, for example, in [11, 12]. Applications of this method range from the study of spatio-temporal dynamics in electrochemical [3, 4, 13], catalytic [14, 15], and reaction-diffusion systems [16-18], flames [19], and hydrodynamic systems [20]. KL decomposition has been used to characterize spatio-temporal chaos [21] and to perform model identification [22] as well.

We consider a spatially extended dynamical system, which is described by a dynamical scalar variable, depending on time and position, $V = V(t, \overrightarrow{r})$. Following a set of measurements, one can assume that these values are known at M instants in time, $V(t_i, \overrightarrow{r}), i = 1, \ldots, M$. The temporal average of this quantity is

$$\langle V(t, \overrightarrow{r})\rangle = \frac{1}{T}\int_0^T V(t, \overrightarrow{r})dt = \frac{1}{M}\sum_{i=1}^{M} V(t_i, \overrightarrow{r}) \quad (7)$$

This is subtracted from the dynamical variable,

$$v(t, \overrightarrow{r}) = V(t, \overrightarrow{r}) - \langle V(t, \overrightarrow{r})\rangle \quad (8)$$

resulting in a quantity with a time average equal to zero. Thus, the method considers only time dependent patterns. The KL decomposition expresses this quantity as a superposition.

$$v(t, \overrightarrow{r}) = \sum_i a_i(t)\phi_i(\overrightarrow{r}) \quad (9)$$

where the set of time dependent amplitude coefficients a_i is orthogonal, and the set of basis space dependent functions, ϕ_k, called alternatively as coherent structures, KL modes or empirical eigenfunctions [19], is orthonormal. It follows that the temporal amplitudes can be obtained by projecting the data set on the eigenfunctions. The orthogonal decomposition (9) is proper, meaning that the average truncation error is at a minimum value [19].

In practice, the value of v is known just in N points of space, as a result of spatial discretisation process. Based upon this, one can define the spatial correlation matrix, by

$$R_{ij} = \frac{1}{T}\int_0^T v(t, \overrightarrow{r_i})v(t, \overrightarrow{r_j})dt \quad (10)$$

The empirical eigenfunctions are the eigenvectors of the spatial correlation matrix R defined by (10) [11]. The application of the above mentioned operations constitute the *direct method* to perform KL decomposition.

The method of snapshots

In a real life application, the use of the direct method can be prohibitive in terms of memory storage and especially of the CPU time. We consider again the instantaneous values corresponding to the dynamical variable,

$$V = V(t_i, \overrightarrow{r_j}), \quad i = 1, \ldots, M; \; j = 1, \ldots N \quad (11)$$

A given value of i corresponds to a *snapshot*. Usually several hundreds of snapshots would provide an accurate description of the dynamics. Based on the snapshots (11), the temporal correlation matrix can be calculated,

$$K_{ij} = \frac{\int_D v(t_i, \overrightarrow{r})v(t_j, \overrightarrow{r})d\overrightarrow{r}}{M\int_D d\overrightarrow{r}} \quad (12)$$

where D denotes the spatial domain. Then, the following eigenproblem can be solved,

$$KA^i = \lambda_i A^i, \quad i = 1, \ldots, M \quad (13)$$

The eigenvectors allow the calculation of the empirical eigenfunctions,

$$\phi_n(\overrightarrow{r}) = \sum_{i=1}^{M} A_i^n v(t_i, \overrightarrow{r}) \quad n = 1, \ldots, M \quad (14)$$

The temporal amplitudes are calculated projecting the data set on the eigenfunctions. This is the *method of snapshots* [11], which leads to a more tractable situation from the computational point of view. The eigenvalues resulted from the solution of (13) are normalized and arranged in descending order:

$$E_i = \frac{\lambda_i}{\sum_{j=1}^{M}\lambda_j} \quad (15)$$

The resulting values of E_i are called energies, because they indicate the contribution of each KL mode in the dynamics. These values allow us to define [19]:

- the KL dimension, D_{KL}, that gives the number of modes that carry a given energy, for example 99% of the total energy. An increase in the number of dynamical degrees of freedom will be reflected in a larger value of D_{KL}. This dimension permits an accurate reconstruction of the dynamics, using the truncation of the development from Eq. (9).
- the KL entropy,

$$S_{\mathrm{KL}} = -\lim_{M\to\infty}\frac{1}{\ln M}\sum_{i=1}^{M} E_i \ln E_i \quad (16)$$

A value of the KL entropy close to zero means that the energy is concentrated on one or few modes, while a value close to one would imply a large number of modes, corresponding for example to chemical or hydrodynamic turbulence [3, 4]. In analogy to hydrodynamic turbulence, such a state is called spatio-temporal turbulence, when correlation both in space and time is very low.

B. Hilbert transform

According to Pikovsky et al. [23], the definition of the phase for an oscillating system is not unique. The Hilbert transform provides a way to calculate the phase and amplitude for such a system [24, 25]. This approach is quite valuable especially in characterizing a type of spatio-temporal chaos, which can be described in terms of phase defects [13]. References [3, 4, 13] present applications of this method in case of electrochemical systems, [26] applies the same approach to describe spatio-temporal dynamics in a catalytic system, and [6, 7] employs the method for an array of electrochemical oscillators.

As the starting point, we consider the dynamical variable according to Eq. (11). On a disk WE, the position can be described using the circular coordinates (r, θ). After subtraction of the time average, the Hilbert transform is calculated as follows [24]:

$$\tilde{v}(t, r, \theta) = \frac{1}{\pi} \int_{-\infty}^{\infty} \frac{v(t', r, \theta)}{t - t'} dt' \qquad (17)$$

The *analytical signal* ξ is defined by:

$$\xi(t, r, \theta) = v(t, r, \theta) + i\tilde{v}(t, r, \theta) \qquad (18)$$

The instantaneous state of the dynamical system can be tracked in the phase space $(v, \tilde{v})$, using the phase and the amplitude defined as:

$$\begin{cases} \varphi = \arg \xi \\ A = |\xi| \end{cases} \qquad (19)$$

A histogram displaying the probability distribution of the phase shift values between oscillators can also characterize the synchronization [7].

In practical implementations, the Hilbert transform is not calculated by Eq. (17). Instead, first the forward Fourier transform of the scalar time series is computed, and then the imaginary part is shifted by $\pi/2$. Finally, the backward Fourier transform provides the Hilbert transform.

3 RESULTS AND DISCUSSION

A. Ring working electrode

Ring working electrodes were used to study experimentally and theoretically the dynamics for a variety of electrocatalytic and metal electrodissolution reactions [1, 2, 13, 27-29]. Numerical simulations to model metal electrodissolution of a ring electrode in 3D electrolyte were done by Birzu et al. [30], in a modeling approach similar to that presented below. The model parameter values we used to model this type of experiments are such that the point-like system corresponding to Eqs. (3), (4) and (6) would be in an oscillatory state: $V_{\mathrm{apl}} = -0.27$ V; $\sigma = 5 \cdot 10^{-5} \Omega^{-1}\mathrm{cm}^{-1}$; $C_{\mathrm{DL}} = 10\ \mu\mathrm{F/cm}^2$; $F_1 = 0.25$ V; $F_2 = 12$ V; $\alpha = 250$; $[\mathrm{H}^+]_{\mathrm{bulk}} = 1.2$ M; $\mu = 5 \cdot 10^{-3}\,\mathrm{cm}^2\mathrm{V}^{-1}\mathrm{s}^{-1}$; $\delta = 0.01$ cm; $D = 5 \cdot 10^{-6}\,\mathrm{cm}^2\mathrm{s}^{-1}$; circumference of the WE, $L_{\mathrm{WE}} = 20$ cm; height of the cell $h = 1$ cm; vertical position of the RE, $z_{\mathrm{RE}} = 0.9$ cm; $A = 5 \cdot 10^{-3}$ mA cm^{-2}. Using these parameter values with a ring WE in a cell depicted in Figure 1a, a rotating pulse is obtained (not shown): an active area travels around the WE at constant speed, total current at the WE being constant. The maintenance of such strongly nonuniform potential drop distribution across the WE is a typical consequence of a negative global electrochemical coupling generated by the point RE [1, 2]: while a region on the WE becomes active, the other regions tends to stay passive. The rotation of the pulse is a result of the positive nonlocal coupling: an active region tends to propagate over the WE. The eigenfunctions corresponding to a simple rotating pulse are usually a pair of sine and cosine functions: a mode composing such a pair is a standing wave. Through KL decomposition we found that for the rotating pulse mentioned above, 95% of the total energy is contained in 4 modes, 80% of the energy being in the first two modes, and the KL entropy is quite low, of 0.378. The modes 3 and 4 are also a sine/cosine pair, of higher order.

The range of the nonlocal electrochemical coupling is given by geometrical aspect ratios like $z_{\mathrm{RE}}/\rho_{\mathrm{WE}}$ or h/ρ_{WE}, while the coupling strength is given by the electrolyte conductivity σ. As a result, decreasing σ, the pattern preserves some features but becomes more irregular. For $\sigma = 4.1 \cdot 10^{-5} \Omega^{-1}\mathrm{cm}^{-1}$, a complex pulse with variable shape and speed rotates on the ring WE (Fig. 2a). On the ring, there are some ‘interruption’ points, where the amplitude of the pulse strongly decreases. These points propagate on the ring on the same direction as the pulse. The number of active modes increases, 95% of the total energy being contained in 8 modes (Fig. 2b), and the KL entropy being 0.467. The first two pairs of eigenfunctions keep the sine/cosine dependence, while the total current is almost periodic, slightly irregular (not shown). Total current is slightly irregular (Fig. 2c).

A further decrease in the conductivity value, to $\sigma = 2.5 \cdot 10^{-5} \Omega^{-1}\mathrm{cm}^{-1}$, leads to an irregular rotating pulse: an active pulse of variable amplitude, shape and speed travels around the ring WE. Sometimes, the direction of propagation reverses (Fig. 3a). The number of active KL modes carrying 95% of the energy doubles again to 16, while the KL entropy increases to 0.569.

The modes appear in pairs of comparable energies – a reminiscence of the rotating pulse – although the eigenfunctions exhibit strong distortions with respect to sine/cosine (not shown).

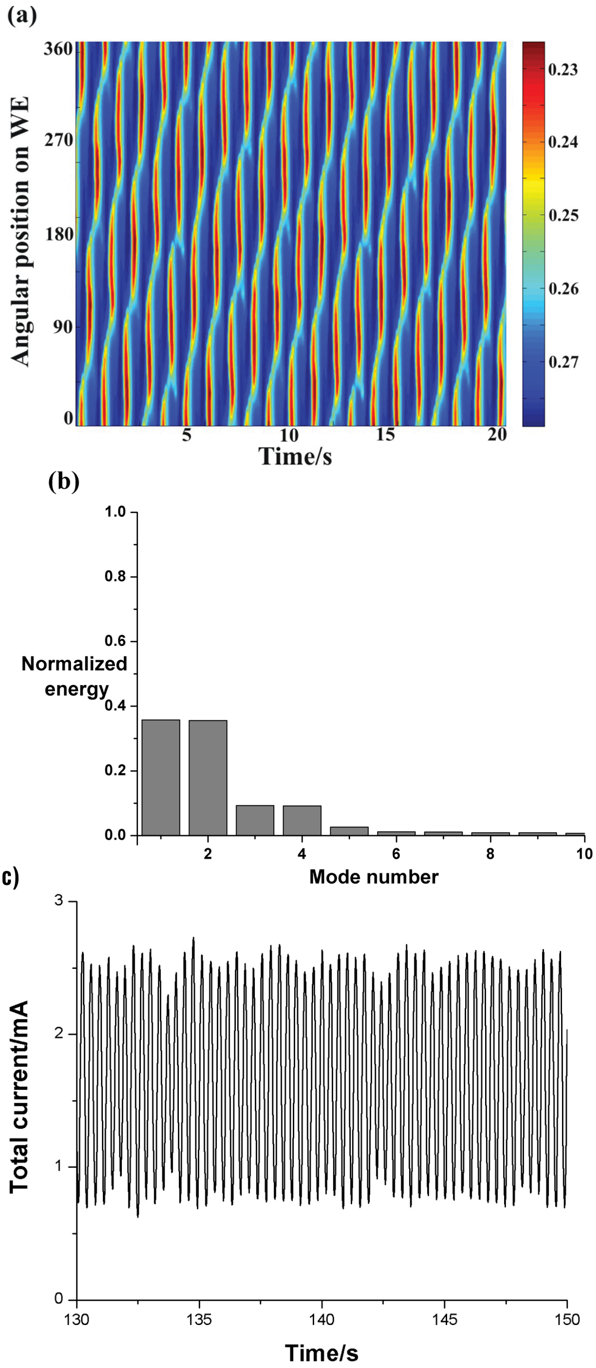

Figure 2 – Complex rotating pulse. **(a)** Spatio-temporal evolution of ϕ_{DL}, red being active and blue being passive; **(b)** KL energy distribution; **(c)** Total current function of time.

At certain moments and points, the amplitude, computed here using the Hilbert transform, goes to zero (Fig. 3b). In such points, the phase is no more well defined and presents a discontinuity (Fig. 3c), the process being called phase defects. Theoretically, in such points the phase gradient goes to infinity. This phenomenon appears in the case of the defect turbulence. A situation similar to that from Figure 3 was studied experimentally by Krischer on a ring WE [13]; there the system undergoes a transition from periodic oscillations to defect turbulence. The total current is chaotic (Fig. 3e).

A further decrease of the conductivity to $\sigma = 2 \cdot 10^{-6}\Omega^{-1}\mathrm{cm}^{-1}$ and respectively of the reaction current to $A = 1.1 \cdot 10^{-3}\mathrm{mA\ cm}^{-2}$ leads to a fully turbulent regime (Fig. 4a). The number of active KL modes carrying 95% of the energy grows to 19, while the KL entropy increases to 0.741. The modes do not group anymore in pairs (Fig. 4b) and the eigenfunctions are irregular (not shown). With respect to the situation depicted in Figure 3, the characteristic correlation length and time decrease: if two points are distant enough in time and/or space they become eventually completely uncorrelated. From Figures 4c to 4e, is apparent the significant increase in the number of phase defects, a signature of fully developed turbulence. Figure 4f displays time dependence of total current, which is chaotic.

In a series of papers, Krischer and coworkers studied experimentally hydrogen oxydation on a ring platinum electrode, in presence of adsorbing ions [13, 27-29]. The variety of obtained patterns is high, including irregular traveling pulses [27, 29] like those obtained in our simulations, complex clusters [28] due to negative global coupling and spatio-temporal chaos [13]. In the frame of present analysis, references [13, 28] are particularly relevant, as they apply both KL decomposition and the analytical signal approach in order to describe complex patterns, similar to those discussed in our work.

B. Disk working electrode

Details regarding the modeling of a metal disk WE electrodissolution in a 3D cell done through numerical simulations can be found in references [3, 4, 31]. Compared to the ring WE, the disk brings experimental challenges related to potential measurements in front of the WE surface, with acceptable spatial and temporal resolution. The elegant solutions found for this problem rely usually on the fact that potential changes on the WE are accompanied by visible (or optically detectable) changes of the surface properties [1, 2]. To model this situation, we consider now the geometry depicted in Figure 1b. The parameter values are the same as those used at the previous example except for the followings: $\sigma = 2.8 \cdot 10^{-5}\Omega^{-1}\mathrm{cm}^{-1}$; circumference of the WE,

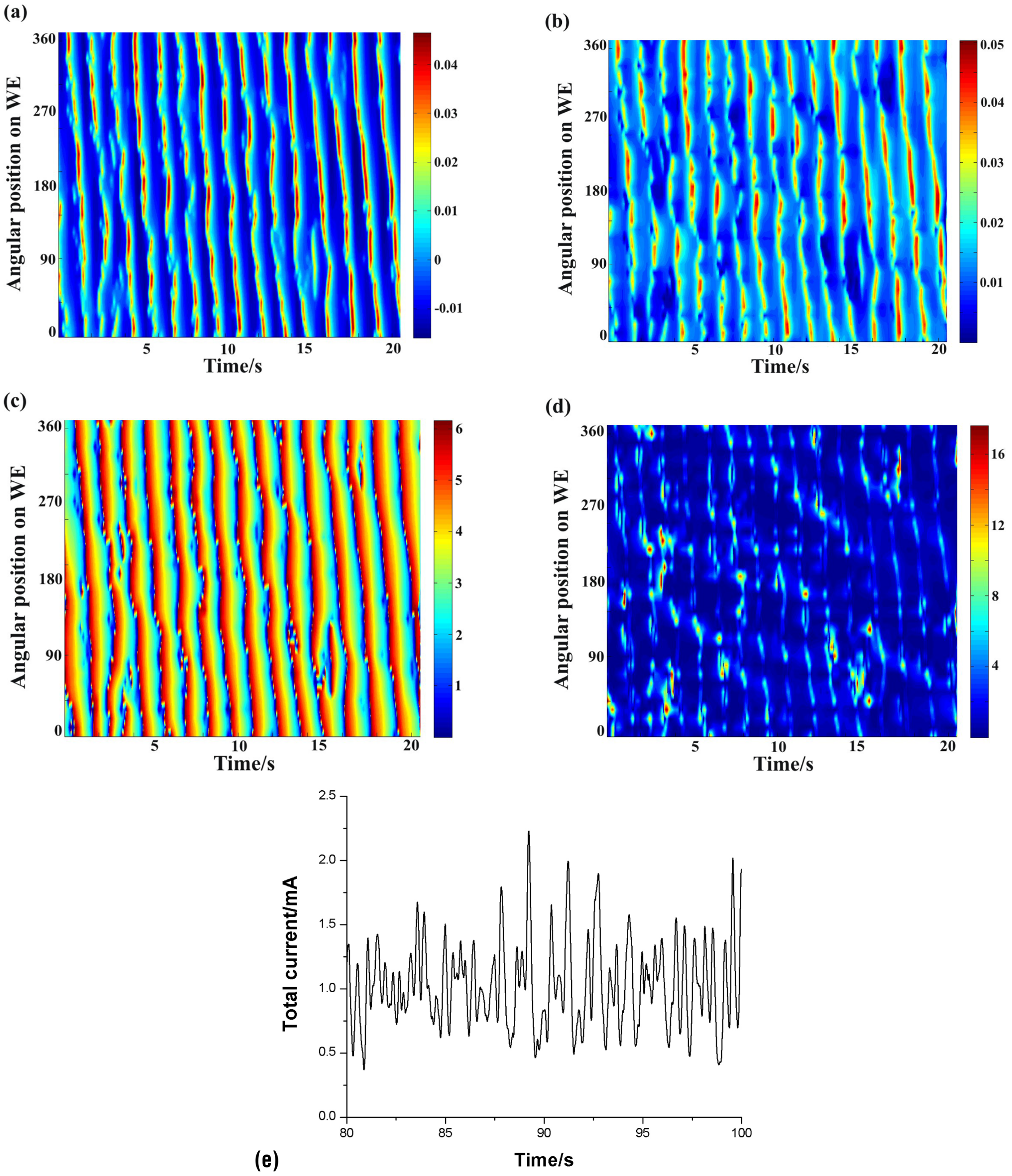

Figure 3 – Irregular rotating pulse. Spatio-temporal evolution of **(a)** $\phi_{\mathrm{DL}} - \langle\phi_{\mathrm{DL}}\rangle$; **(b)** amplitude; **(c)** phase; **(d)** phase gradient; **(e)** total current function of time.

$L_{\mathrm{WE}} = 10$ cm; vertical position of the RE, $z_{\mathrm{RE}} = 0.2$ cm; $A = 2 \cdot 10^{-3}\mathrm{mA\,cm}^{-2}$. For these parameter values, the model results in second mode antiphase oscillations [5]: the electrode exhibits angular symmetric states where four equal sectors of the disk oscillate, forming two synchronized pairs (Fig. 5a). Similar to the case with the rotating pulse, this is a consequence of the negative global coupling induced by the point RE.

Inspecting the evolution described by Figure 5a, it is visible that it is not a simple second mode antiphase oscillation, but it involves several modes. Indeed, the normalized energy distribution (not shown) calculated using the KL decomposition, confirms that only the first three modes are relevant to the overall dynamics, carrying 95% of the energy; the normalized energy of the fourth mode is already under 1%. The KL entropy associated to this dynamics

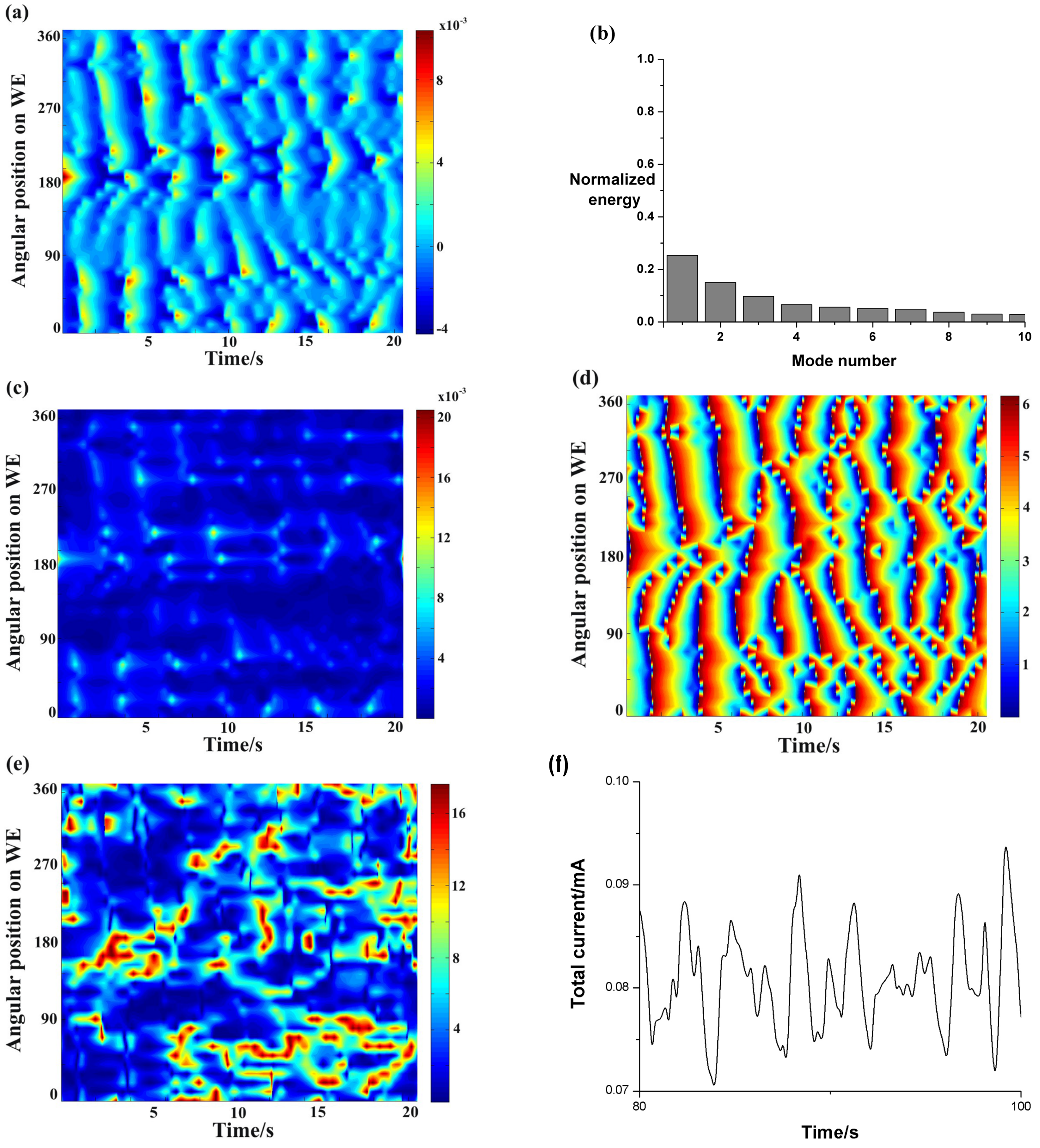

Figure 4 – Spatio-temporal chaos. Spatio-temporal evolution of **(a)** $\phi_{\mathrm{DL}} - \langle\phi_{\mathrm{DL}}\rangle$; **(b)** KL energy distribution; **(c)** amplitude; **(d)** phase; **(e)** phase gradient; **(f)** Total current function of time.

is 0.116, showing that the total number of active modes is low. In Figure 5b, is visible that the first mode is actually associated to a 'pure' second mode antiphase dynamics. In the overall dynamics, two more modes, with higher symmetry, are active. Total current is periodic, with double the frequency of local oscillator (Fig. 5c).

Surprisingly, when the distance between the point RE and the disk WE is increased to 0.7 cm, while the other parameters are kept constant, the dynamics at the WE becomes more complex (Fig. 6). The distance between WE and RE gives the range of the migration coupling at the WE; a larger distance would be expected

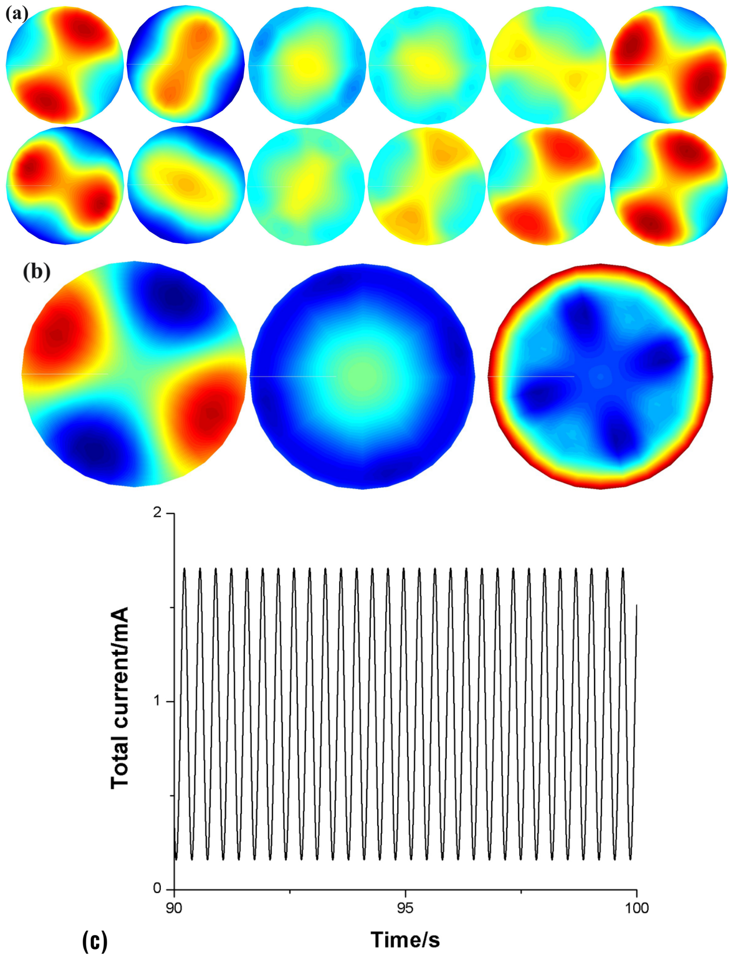

Figure 5 – Second mode antiphase oscillations. **(a)** Snapshots with instantaneous state on the disk WE at different times, over an oscillatory period, red being active and blue being passive; corresponding time values for the individual frames are 50.25, 50.35, 50.45, 50.47, 50.51, 50.60, 50.65, 50.73, 50.82, 50.86, 50.90 and 50.94, respectively; **(b)** The first three KL eigenfunctions; **(c)** Total current function of time.

to result in more ordered dynamics. In some respects the dynamics is similar to that shown in Figure 2 for the ring electrode. The snapshots from Figure 6b show that the pattern combines some properties of standing waves and rotating pulses: a pulse with variable shape, amplitude and speed travels around the disk WE. At some 'interruption points' the amplitude strongly diminishes and the active region tends then to occupy the opposite side of the WE. At some moments, these interruption points move around the disk WE, resulting in a modulation of the total current (Fig. 6d). The number of KL modes carrying 95% of the total energy is 5, while the KL entropy is quite low, 0.187. The KL analysis allows us to decipher the properties of this complex dynamics, namely to describe the modes that carry most of its energy. As can be seen in Figure 6c, the first two modes represent a pair of standing waves of almost equal energies, while modes 3 and 4 have high symmetry, the 3rd mode being close to a homogeneous oscillation. Considering the symmetry of the higher modes, they group 5 with 7 and 6 with 8.

Because the current in the upper plane flows just through the ring CE, the geometry from Figure 1b tends to favor strongly nonuniform states at the WE. In order to obtain more uniform distributions, we used cell geometry similar to that from Figure 1b, but now both the RE and CE (situated on the upper plane of the cylindrical cell) are modelled as an equipotential disk. This situation would correspond to an experiment when the RE is beyond the plane of the CE. The parameters are the same as in Figure 2, except $\sigma = 2 \cdot 10^{-6}\Omega^{-1}\mathrm{cm}^{-1}$; circumference of the WE, $L_{\mathrm{WE}} = 150\ \mathrm{cm}$; cell height $h = 2\ \mathrm{cm}$ and $A = 2 \cdot 10^{-4}\mathrm{mA\ cm}^{-2}$. When the conductivity is extremely low and the geometrical aspect ratio is $h/\rho_{\mathrm{WE}} \ll 1$, the coupling is local (diffusive) and weak, resulting in fully developed spatio-temporal turbulence [3].

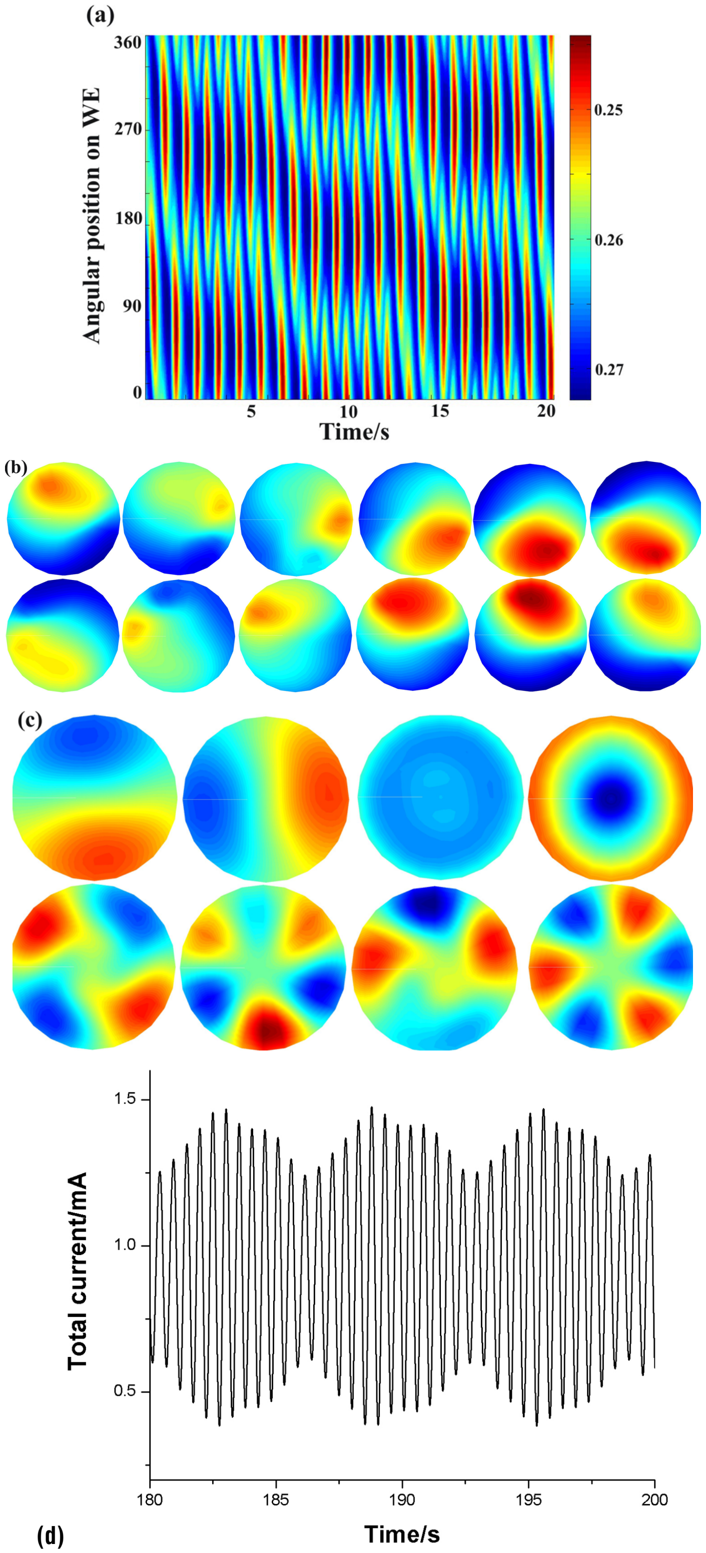

Figure 6 – Complex rotating pulse. **(a)** Spatio-temporal evolution of ϕ_{DL} for a given value of the radius, on the WE; **(b)** Snapshots with instantaneous states on the disk WE at different times, over a short oscillation period, red being active and blue being passive; time values are 90., 90.05, 90.10, 90.15, 90.20, 90.25, 90.30, 90.35, 90.40, 90.45, 90.50 and 90.55, respectively; **(c)** First 8 KL eigenfunctions; **(d)** Total current function of time.

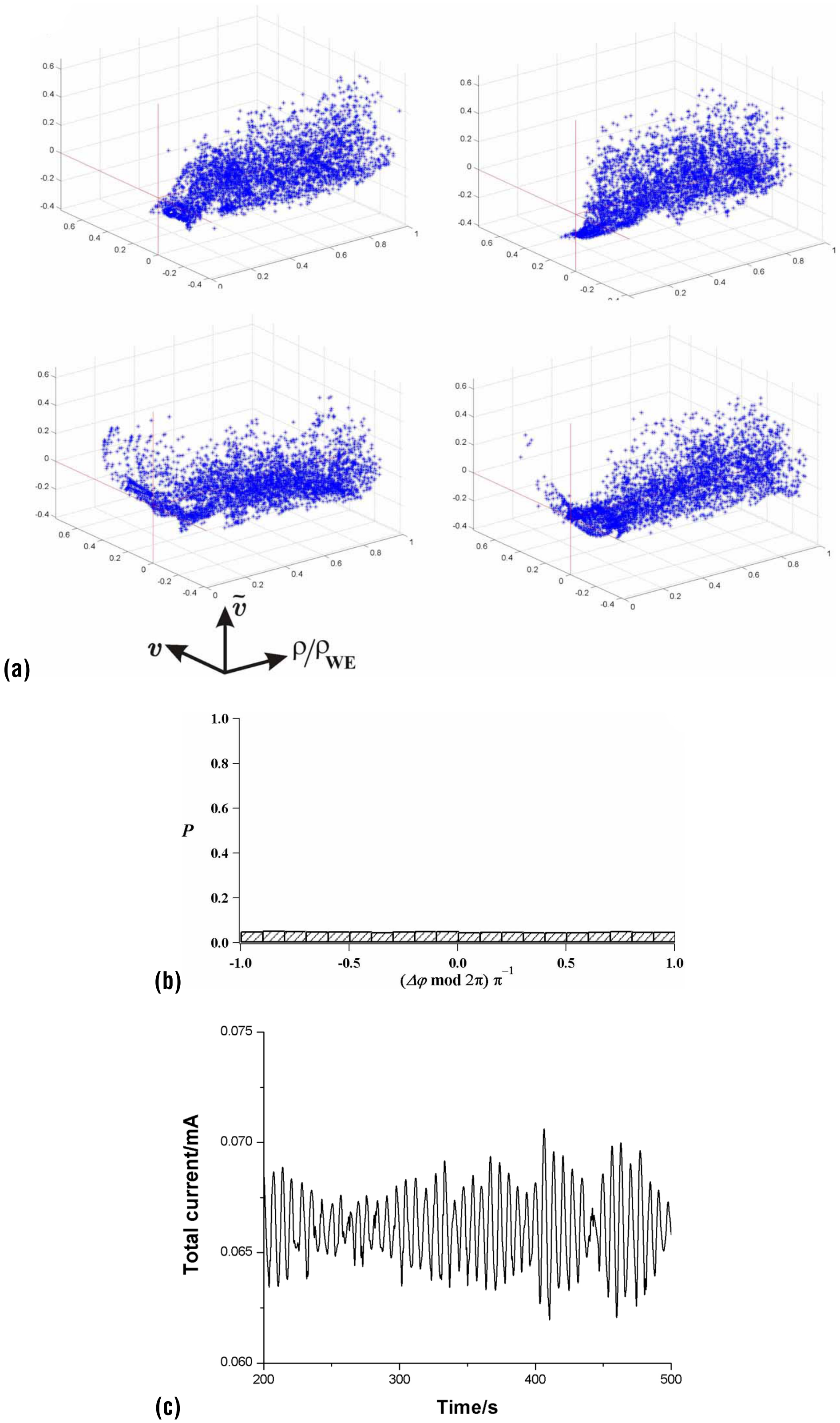

Figure 7 – Spatio-temporal chaos on a disk WE. **(a)** Phase space representation at different times. **(b)** Histogram of the probability of different phase shifts between two oscillators on the WE; **(c)** Total current function of time.

When calculating the KL decomposition, it results that 99.99% of the energy is contained in an extremely large number of modes, namely 959, and the associated KL entropy is 0.693. The normalized energy of the first mode is 8.9%, decreasing slowly for higher modes. With the increase of the mode number, the spatial pattern of the eigenfunctions becomes more and more complex, with a higher irregularity and a lower characteristic space scale. From the snapshots of the phase space representation in Figure 7a, the wide phase space distribution for the points of the WE can be noticed; this reflects the low spatial correlation on the WE. Also, this kind of phase space representation allows to discriminate the properties of the dynamics for different values of the radius ρ on the WE.

Figure 7b shows the histogram of the probability of the phase shift for the turbulent regime. We considered the points on the WE for an intermediate radius, $\rho = \rho_{\mathrm{WE}}/2$. On this intermediate circle, a point was taken as reference, and the phase shifts of other points on the circle were calculated:

$$\Delta\varphi_{1,k} = \varphi_k(t) - \varphi_1(t) \tag{20}$$

Based on these values, the histogram can be calculated. In Figure 7b, the phase shift distribution is almost uniform, illustrating the lack of temporal and spatial correlations, typical for chaotic regimes. The total current is chaotic (Fig. 7c).

While it is much easier to measure experimentally the total current through WE at different times than to monitor the potential in front of WE with spatial and temporal resolution, as it can be seen in all the above mentioned examples, total current gives just limited information about the spatio-temporal pattern at WE.

4 CONCLUSIONS

The simple periodic behaviour of a point-like nonlinear dynamical system may change into extremely complex dynamics under spatially extended conditions. This was demonstrated by modelling metal electrodissolution in 3D electrochemical cells considering both ring and disk working electrodes. Complex patterns like rotating pulses, complex or irregular rotating pulses, high order antiphase oscillations and turbulent states were identified. These patterns were characterized mainly by KL decomposition and Hilbert transform, which are effective tools to characterize dynamical systems. While the first method applies to spatially extended systems, the second approach can be used both for point-like and spatially extended systems, and also for arrays of oscillators.

KL method decomposes a given dynamics into eigenmodes, each being the product of a spatial eigenfunction and temporal amplitude. A normalized energy can be associated to each mode, that makes possible to quantify its contribution to the overall dynamics. This allows the recomposition of the dynamical variable with a prescribed accuracy while simplifying the dynamical description by truncation. Also, based on the normalized energy distribution, the KL dimension and entropy associated to the dynamics can be computed. The values obtained this way show if the dynamics is simple or chaotic (turbulent). However, the efficiency of this method is not limited to nonlinear dynamical system, but it can be used whenever the state of a spatially distributed system changes in time, providing thus a very useful tool in engineering applications.

The Hilbert transform starts from a scalar time series, which then can be described in terms of phase and amplitude. Some applications of this method are:

a) Starting from a scalar time series, the phase portrait can be calculated; for a spatially extended system, one plots a 3D phase portrait that takes into account the spatial variations of the dynamics. This can be used also to obtain an animated phase portrait.

b) For spatially extended dynamical systems, the description in terms of phase and amplitude proves to be extremely useful, especially for spatio-temporal chaos that can be characterized in terms of phase defects.

c) Based on the phase values, the phase shifts between two oscillators can be calculated, and then the histogram of the phase shifts can be created. This also allows the computation of the phase entropy.

ACKNOWLEDGMENTS

A. Bîrzu thanks K. Krischer and I. Kiss for useful discussions and the European Science Foundation for a short mobility grant within the framework of the Research Network Programme FUNCDYN. V. Gáspár thanks the Hungarian Research Grants OTKA T60417, T81646 and the TÁMOP 4.2.1./B-09/1/KONV-2010-0007 project for financial support. The TÁMOP project is co-financed by the European Union and the European Social Fund.

REFERENCES

[1] KRISCHER K. 1999. Modern Aspects of Electrochemistry, eds. B.E. Conway, J. O'M. Bockris, and R.E. White (Kluwer Academic/Plenum Press, NY, vol. 32).

[2] KRISCHER K. 2002. Advances in Electrochemical Science and Engineering, eds. R.C. Alkire and D.M. Kolb (Wiley-VCH, Weinheim, vol. 8).

[3] BÎRZU A & KRISCHER K. 2006. Phys. Chem. Chem. Phys., 8: 3659.

[4] BÎRZU A & KRISCHER K. 2007. Z. Phys. Chem., 221: 1245.

[5] BÎRZU A, PLENGE F, JAEGER NI, HUDSON JL & KRISCHER K. 2003. J. Phys. Chem. B, 107: 5825.

[6] KISS IZ, ZHAI Y & HUDSON JL. 2002. Science, 296: 1676.

[7] BÎRZU A & GÁSPÁR V. 2009. Electrochim. Acta, 55: 383.

[8] STROGATZ SH. 1994. Nonlinear Dynamics and Chaos (Addison Wesley, Reading).

[9] BÎRZU A, GREEN BJ, OTTERSTEDT RD, JAEGER NI & HUDSON JL. 2000. Phys. Chem. Chem. Phys., 2: 2715.

[10] HSL. 2011. A collection of FORTRAN codes for large scale scientific computation. http://www.hsl.rl.ac.uk.

[11] BREUER KS & SIROVICH L. 1991. J. Comp. Phys., 96: 277.

[12] ARMBRUSTER D, HEILAND R & KOSTELICH EJ. 1994. Chaos, 4: 421.

[13] VARELA H, BETA C, BONNEFONT A & KRISCHER K. 2005. Phys. Rev. Lett., 94: 174104.

[14] GRAHAM MD, LANE SL & LUSS D. 1993. J. Phys. Chem., 97: 889.

[15] KRISCHER K, RICO-MARTINEZ R, KEVREKIDIS IG, ROTERMUND HH, ERTL G & HUDSON JL. 1993. AICHE. J., 39: 89.

[16] MEIXNER M, ZOLDI SM, BOSE S & SCHÖLL E. 2000. Phys. Rev. E, 61: 1382.

[17] BAGYAN S, MAIR T, SUCHORSKI Y, HAUSER MJB & STRAUBE R. 2008. J. Phys. Chem. B, 112: 14334.

[18] TRIANDAF I & SCHWARTZ IB. 1997. Phys. Rev. E, 56: 204.

[19] PALACIOS A, GUNARATNE GH, GORMAN M & ROBINSON KA. 1998. Phys. Rev. E, 57: 5958.

[20] CIZMAS P, PALACIOS A, O'BRIEN T & SYAMLAL M. 2003. Chem. Eng. Sci., 58: 4417.

[21] ZOLDI SM & GREENSIDE HS. 1997. Phys. Rev. Lett., 78: 1687.

[22] QI C & LI HX. 2008. Ind. Eng. Chem. Res., 47: 4184.

[23] PIKOVSKY AS, ROSENBLUM MG, OSIPOV GV & KURTHS J. 1997. Phys. D, 104: 219.

[24] ROSENBLUM M & KURTHS J. 1998. Nonlinear Analysis of Physiological Data, eds. H. Kantz, J. Kurths, G. Mayer-Kress (Springer, NY, p. 91).

[25] PIKOVSKY A, ROSENBLUM M & KURTHS J. 2001. Synchronization: a universal concept in nonlinear sciences (Cambridge University Press).

[26] BERTRAM M, BETA C, POLLMANN M, MIKHAILOV AS, ROTERMUND HH & ERTL G. 2003. Phys. Rev. E, 67: 036208.

[27] GRAUEL P, VARELA H & KRISCHER K. 2001. Faraday Discuss., 120: 165.

[28] VARELA H, BETA C, BONNEFONT A & KRISCHER K. 2005. Phys. Chem. Phys., 7: 2429.

[29] PLENGE F, VARELA H & KRISCHER K. 2005. Phys. Rev. Lett., 94: 198301.

[30] BÎRZU A, GREEN BJ, JAEGER NI & HUDSON JL. 2001. J. Electroanal. Chem., 504: 126.

[31] BÎRZU A, GREEN BJ, OTTERSTEDT RD, HUDSON JL & JAEGER NI. 2002. Z. Phys. Chem., 216: 1.